Behavior of Deconstructable Steel-Concrete Shear Connection in Composite Beams

Lizhong Wang[1]; Mark D. Webster[2]; and Jerome F. Hajjar[3]

[1] Graduate Research Assistant, Department of Civil and Environmental Engineering, Northeastern University, Boston, MA 02115. E-mail: wang.l@husky.neu.edu
[2] Senior Staff II – Structures, Simpson Gumpertz & Heger Inc., Waltham, MA 02453. E-mail: MDWebster@sgh.com
[3] CDM Smith Professor and Chair, Department of Civil and Environmental Engineering, Northeastern University, Boston, MA 02115. E-mail: JF.Hajjar@neu.edu

Abastrct

A new deconstructable composite floor system consisting of precast concrete planks and deconstructable clamping connections is proposed to promote sustainable design of composite floor systems within steel buildings through comprehensive reuse of all key structural components. A pushout test setup has been developed to study the clamping connector behavior experimentally. Finite element analysis results are presented to investigate the strength and ductility of the deconstructable shear connectors and study the effects of the analysis parameters. The scope of the project also includes beam and diaphragm tests to study the flexural and in-plane behavior of the structural system.

INTRODUCTION

According to the U.S. Department of Energy Buildings Energy Data Book, construction and use of commercial and residential buildings in the United States accounted for approximately 40% of U.S. energy consumption in 2009, while the industrial sector and the transportation sector each accounted for an additional 30% (Energy Information Administration 2009). Currently, the "use" phase of the buildings consumes the largest quantities of natural resources and creates the greatest environmental impacts, but the construction and demolition of the buildings will hold a larger proportion as new technologies are developed to increase operational efficiencies.

The need to reduce the energy consumption and material waste related to the construction industry motivates the exploration of Design for Deconstruction (DfD) of buildings. DfD aims to increase the quantity of materials recovered from renovation and demolition projects so that they can be reused with little or no refabrication in new construction projects. Contrary to the conventional linear material flow, which starts with the extraction of raw materials and ends with the disposal of debris in landfills, DfD could help close this loop by reducing the cost of recovering and reusing resources.

Steel-concrete composite floor framing systems make the most efficient use of the two materials, with concrete being subjected to compressive forces and steel resisting tensile forces, providing a cost-effective solution. However, traditional composite concrete floor slabs are poured integrally with the supporting steel framing systems, inhibiting the separation of the two materials. Steel beams can be recycled, and concrete slabs can be crushed for fill or making aggregates for new concrete, but these components cannot be reused.

This paper introduces a new deconstructable composite floor system that enables sustainable design of composite floor framing in steel building structures and reuse of the structural components. A pushout test setup has been designed to establish the clamping connector performance experimentally. Finite element models have also been developed to investigate the behavior of the clamping connectors analytically. The scope of this ongoing project also includes beam and diaphragm tests to study the flexural and in-plane behavior of the structural system.

DECONSTRUCTABLE COMPOSITE FLOOR SYSTEM

The prototype for a deconstructable composite beam prototype is shown in Figure 1. The system includes precast concrete floor planks that are clamped to the girders and beams to achieve composite action in the flooring system. Cast-in channels are embedded in the concrete planks to provide flexibility for where the beam intersects the plank and to allow for different beam widths. Bolts are pretensioned to firmly clamp the steel beam and the concrete plank together, thus generating frictional forces at the steel-concrete interface.

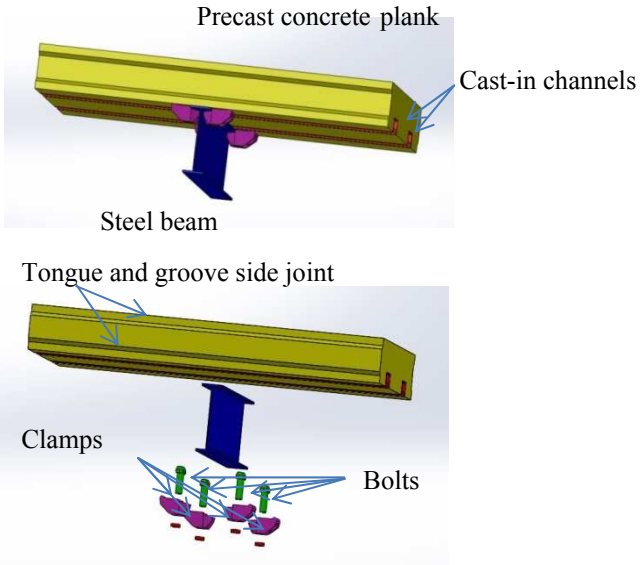

Figure 1. Deconstructable composite beam prototype

Preliminary dimensions of the plank, presented in Figure 2, are 20 ft. × 2 ft. × 6 in. This provides a plank size that is large enough to have structural integrity but small enough to facilitate handling and to promote reconfiguring the planks in future

structures. The connections between adjacent planks to resist in-plane diaphragm forces are still under design. The configuration in Figure 1 includes a tongue and groove mating edge that ensures the adjacent planks share shear load and offers a level and well-matched surface. A typical plan layout for an office building using this system is shown in Figure 3.

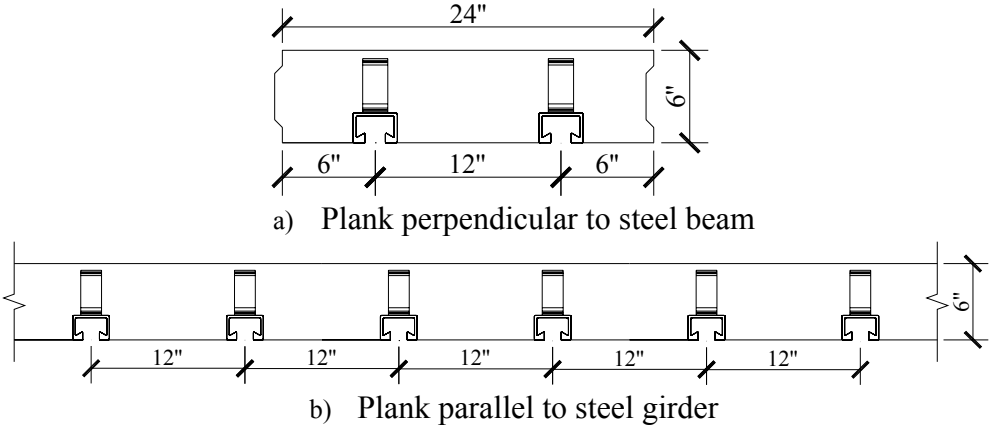

Figure 2. Precast concrete plank cross section (units: inches)

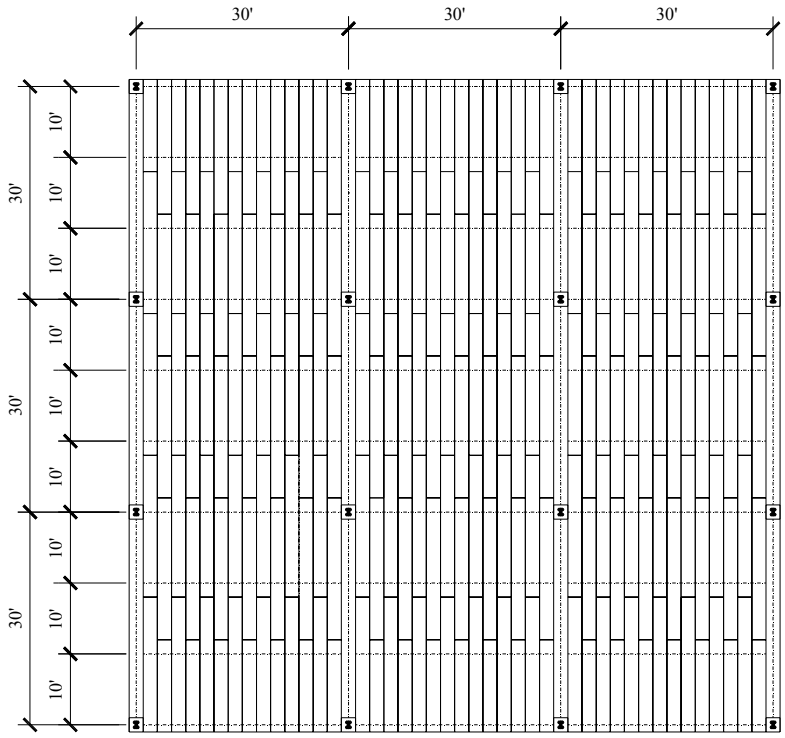

Notes:
1. The dashed lines show the steel framing. The beams are perpendicular to the precast concrete planks, while the girders are parallel to the planks.
2. Other precast plank patterns are also possible for the DfD system.

Figure 3. Typical floor plan for deconstructable composite floor systems (units: feet)

PUSHOUT TEST SETUP

Numerous pushout test setups have been developed in the past to study the behavior of steel headed stud anchors, see Gattesco et al. (1996), Anderson et al. (2000), Saari et al. (2004) and Lam et al. (2005). Eurocode 4 (CEN 2004) specified a standard test specimen for shear studs embedded in solid slabs, and indicated that the test setup may be adapted to conform to specific detailing of a system.

A new full-scale test setup utilizing a self-reacting frame is illustrated in Figure 4. This test setup can be used for both monotonic and cyclic loading tests. The test specimen consists of a precast concrete plank supporting a WT section. The size of the precast concrete plank is 4 ft. × 2 ft. × 6 in. WT 5x30 and WT 4x15.5 are selected to represent different potential sizes of girders, with the smaller WT requiring shims between the clamp and the WT flange since the flange is relatively thin, as may be typical in smaller floor beams. The stem of the WT at the end of the member that attaches to the actuator is coped to ensure that the actuator load is applied only to the flanges to reduce eccentricity of the force application in the WT. Reaction angles are chosen to react against the concrete plank to provide realistic compressive stress distributions within the concrete. ASTM 992 steel is used for the WT sections, while A36 steel is selected for the reaction angle sections and the plates that constitute the remainder of the load frame. The whole test setup is restrained vertically, as separation of the concrete slab and the steel beam is rarely seen in composite beams.

Two reinforcement patterns are designed for the pushout test specimens, see Figure 5. The heavy reinforcement pattern includes supplementary reinforcement that bridges all potential concrete failure planes to restrain the opening and propagation of the cracks. The light reinforcement pattern, which only retains the bars designed for gravity loading and eliminates some of the shear reinforcement, is used for specimens where premature concrete failure is anticipated to explore this limit state. The spacing of the channel anchors is 9.65 in. (245 mm), which is equal to that for the transverse reinforcement and vertical reinforcement in the light reinforcement pattern. In the heavy reinforcement pattern, the reinforcement spacing decreases as close to the clamping connectors to provide extra protection against concrete breakout.

In this work, full-scale composite beam tests are planned to study realistic behavior of the clamping connections. In addition, the seismic performance of a deconstructable composite flooring system will be established in full-scale diaphragm tests to address the in-plane force transfer of the diaphragm system. Preliminary test setups for the full-scale beam tests and in-plane diaphragm tests are provided in Figure 6.

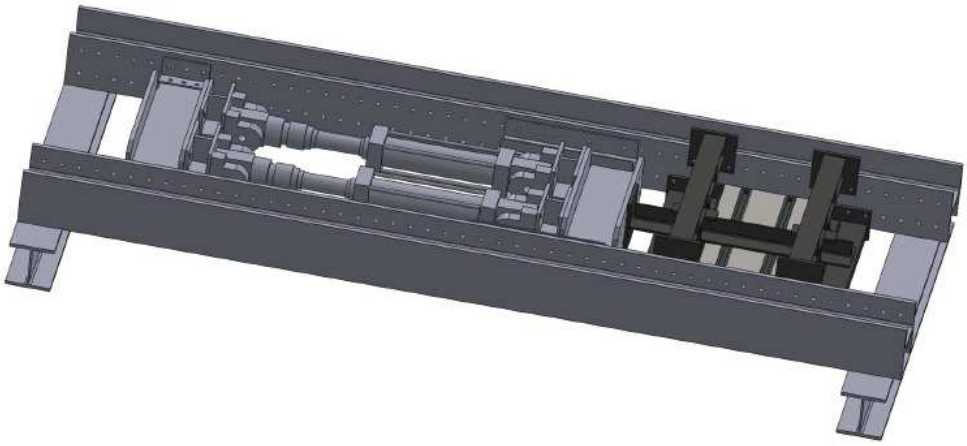

a) Test rig

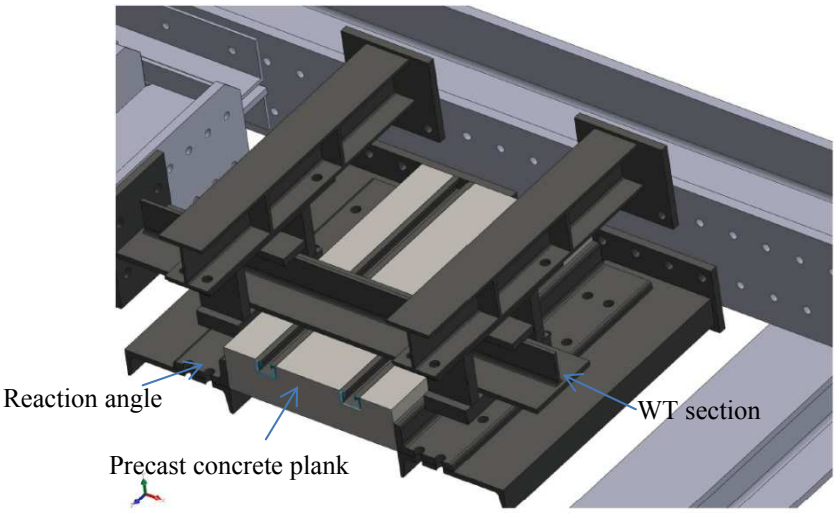

b) Cross section view

Figure 4. Pushout test specimen for the clamping connectors

1) Elevation view

2) Side view

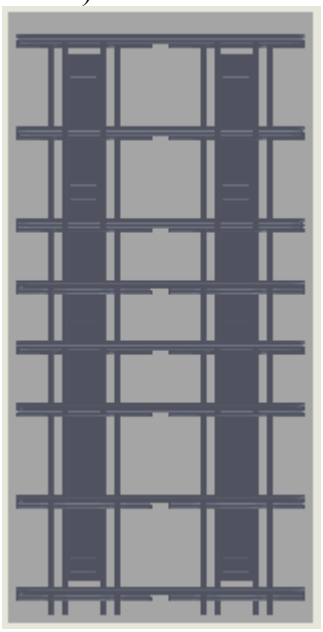

3) Plan view

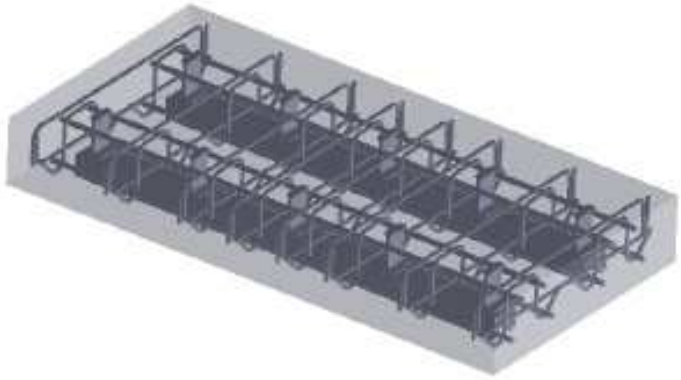

4) Three-dimensional view

a) Heavy reinforcement pattern

1) Elevation view

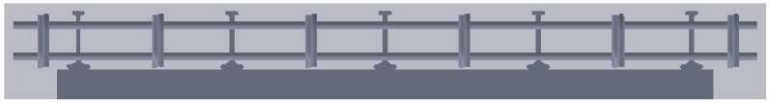

2) Side view

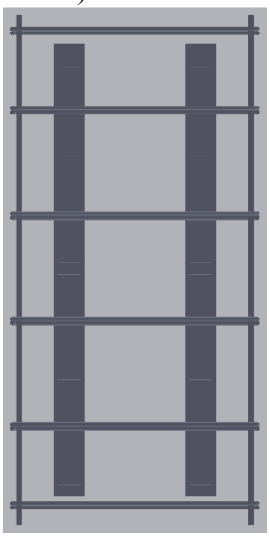

3) Plan view

4) Three-dimensional view

b) Light reinforcement pattern

Figure 5. Reinforcement patterns

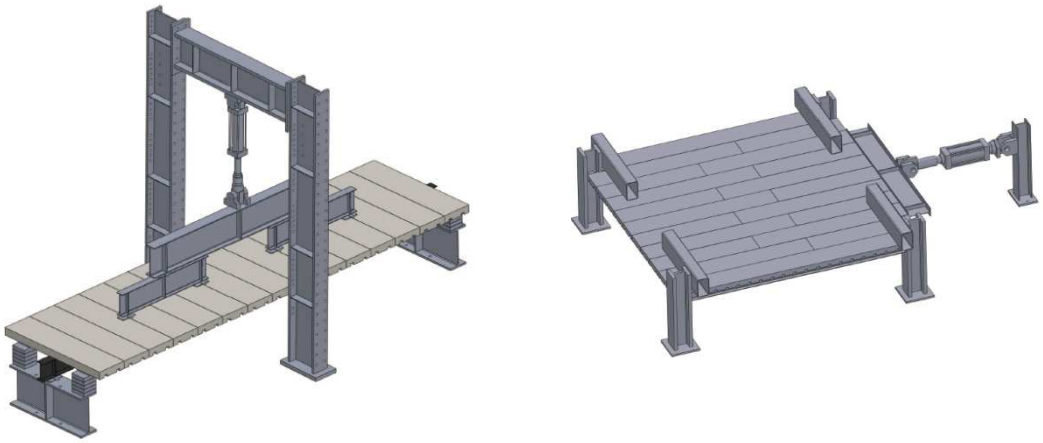

a) Beam tests b) Diaphram tests

Figure 6. Beam tests and diaphragm tests

PRELIMINARY FINITE ELEMENT ANALYSIS RESULTS

Finite element analysis is conducted to examine potential limit states in the pushout tests and assist specimen design. All finite element models are developed in Abaqus/CAE and analyzed using Abaqus/Explicit, which is effective for simulations containing material failure and contact (Abaqus 2012). This procedure can be used for quasi-static problems if the loads are applied sufficiently slowly.

Finite element model and mesh. Cast-in channels are meshed with both eight-node reduced integration brick elements (C3D8R) and six-node reduced integration triangular prism elements (C3D6R). Steel beams and concrete plank are meshed with C3D8R only. Due to the complex geometry of the clamps and the bolts, four-node tetrahedron elements (C3D4) are employed. Reinforcement is modelled using two-node three-dimensional truss elements (T3D2).

Boundary conditions and load applications. The boundary conditions for the model are shown in Figure 7. A symmetric boundary condition is defined such that nodes on these surfaces are prevented from translating in the Z direction and rotating in the X and Y directions.

Two steps are defined for the loading process. Pretension is first applied by assigning a thermal expansion coefficient and temperature change to the clamping bolts, creating thermal shrinkage in the bolt and generating tensile forces in the bolt shank because of the constraints at the bolt ends. The steel beam flange is then loaded in the X direction using displacement control. In order to obtain a quasi-static solution, it is essential to apply the loading slowly and smoothly to minimize dynamic effect. An optimal loading rate is found to be 0.1 mm/s.

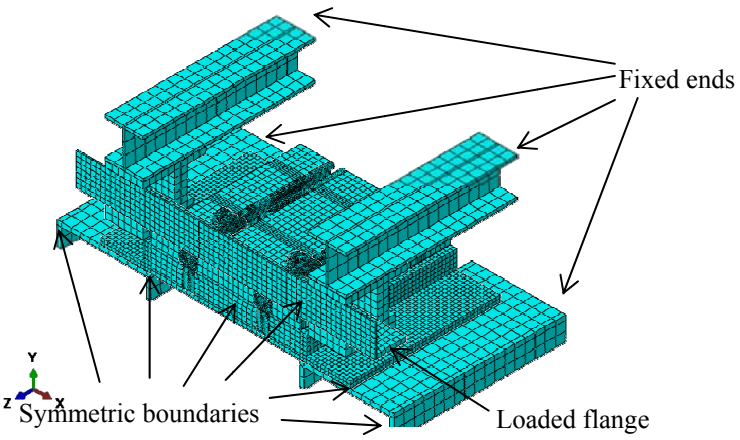

Figure 7. Meshed assembly and boundary conditions

Material model for concrete. A concrete damage plasticity model is used to model the concrete plank. Two main failure mechanisms are assumed for this material model: tensile cracking and compressive crushing. Under uniaxial tensile loading, the stress-strain curve displays a liner elastic relationship until the cracking stress is reached. The formation of cracking leads to a softening stress-strain curve afterwards. Under uniaxial compressive loading, the stress-strain curve is linear and elastic until the value of initial yield. The curve is then followed by strain hardening and strain softening beyond the ultimate stress. These relations are presented in the equations below. Under cyclic loading, it can model opening and closing of cracks observed in tests by allowing for stiffness recovery when the load is reversed. The tensile and compressive stress-strain curves in the Chinese Code for Design of Concrete Structures (GB 50010-2002 2002; Pavlović et al. 2013) are used for this analysis, as shown in the equations below, respectively. These constitutive relationships define uniaxial concrete strength at high strains, which may occur in the vicinity of the embedded channels. The elastic modulus and Poission's ratio are taken as 30 GPa and 0.2, respectively.

$$\sigma_c = \begin{cases} f_c\left(\alpha_a\left(\frac{\varepsilon}{\varepsilon_c}\right) + (3-2\alpha_a)\left(\frac{\varepsilon}{\varepsilon_c}\right)^2 + (\alpha_a - 2)\left(\frac{\varepsilon}{\varepsilon_c}\right)^3\right) & \frac{\varepsilon}{\varepsilon_c} \le 1 \\ \dfrac{\frac{f_c\varepsilon}{\varepsilon_c}}{\alpha_d\left(\frac{\varepsilon}{\varepsilon_c} - 1\right)^2 + \frac{\varepsilon}{\varepsilon_c}} & \frac{\varepsilon}{\varepsilon_c} > 1 \end{cases}$$

$$\sigma_t = \begin{cases} f_t\left(1.2\left(\frac{\varepsilon}{\varepsilon_t}\right) - 0.2\left(\frac{\varepsilon}{\varepsilon_t}\right)^6\right) \le 1 & \frac{\varepsilon}{\varepsilon_t} \le 1 \\ \dfrac{\frac{f_t\varepsilon}{\varepsilon_t}}{\alpha_t\left(\frac{\varepsilon}{\varepsilon_t}\right)^{1.7} + \frac{\varepsilon}{\varepsilon_t}} & \frac{\varepsilon}{\varepsilon_t} > 1 \end{cases}$$

where ε_t and ε_c are strains corresponding to the peak stresses, f_t and f_c, respectively; α_a ,α_d and α_t are coefficients obtained from test results. The uniaxial compressive stress-strain curve for C30 (f_c'= 30 MPa) concrete is depicted in Figure 7.

Concrete damage plasticity parameters used in this formulation as specified in ABAQUS (2012) include: dilation angle= 38°, eccentricity = 0.1. K_c, the ratio of the second invariant of the stress deviator on the tensile meridian to that on the compressive meridian at initial yield at a given first invariant of stress such that the maximum principal stress is negative, is equal to 0.67. The ratio of biaxial compressive yield stress to uniaxial compressive yield stress σ_{b0}/σ_{c0} is taken as 1.16.

Concrete damage variables are also defined, such that softening due to damage initiates when the strains exceed those corresponding to the peak stresses, thus bringing the damage parameters to zero. Concrete tensile damage D_t and compressive damage D_c are derived using the following expressions:

$$D_t = 1 - \sigma_t/f_t$$

$$D_c = 1 - \sigma_c/f_c$$

Material model for steel beam, rebar, channels and bolts. Elastic-perfectly-plastic material is defined for the steel beam, reinforcement, and channels. The nominal yield stress for steel beam and channels is taken as 345 MPa, and the nominal yield stress is 400 MPa for the reinforcement. The elastic modulus is taken as 200 GPa for all of these components. The mechanical behavior is assumed to be the same in both tension and compression. A typical stress-strain curve for Grade 8.8 bolt material is provided in Kulak et al. (1987) and used for the analysis, as seen in Figure 8b.

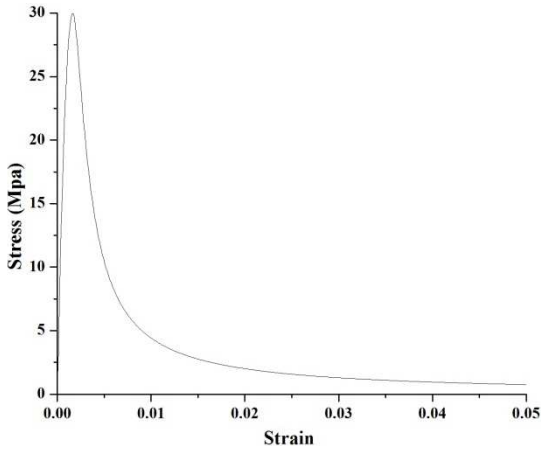

a) C30 concrete compressive behavior

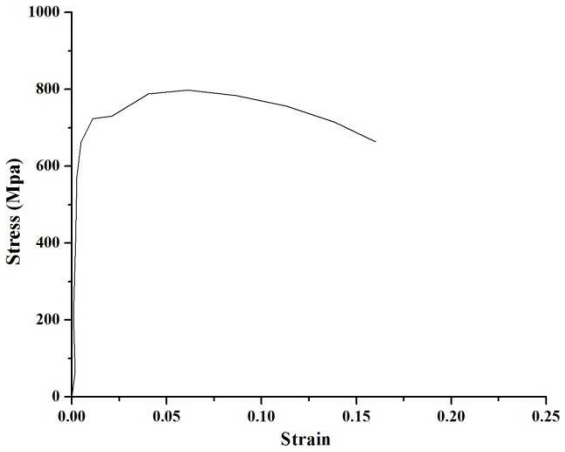

b) Bolt material

Figure 8. Material stress-strain curves

Analysis results. Table 1 lists the parameters that were used for the computational models, which include the loading protocol, the usage of shims for the clamps, the

amount of bolt pretension, and the different reinforcement patterns. The monotonic and cyclic loading protocols are provided in Figure 9. Large pretension and small pretension are defined as 85% and 70% of the minimum tensile strength of the bolts, respectively.

Table 1. Parameters for the computational models

Model Number	Loading protocol	Usage of shim	Amount of bolt pretension	Reinforcement pattern
1	Monotonic	No	Small	Heavy
2	Monotonic	No	Small	Light
3	Monotonic	No	Large	Heavy
4	Monotonic	Yes	Small	Heavy
5	Cyclic	No	Small	Heavy

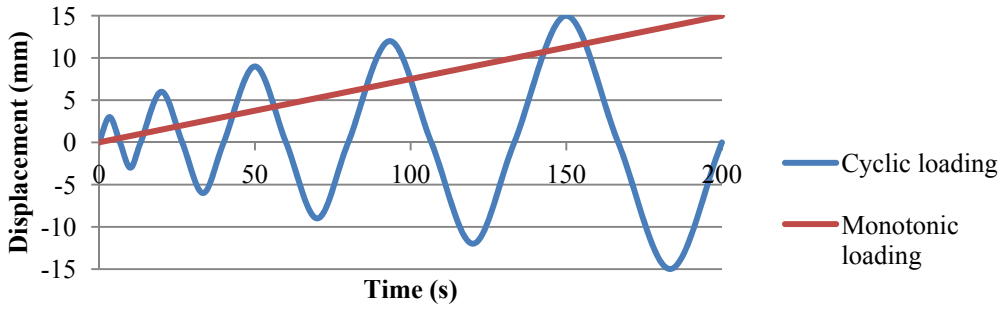

Figure 9. Loading protocols for the computational models

The load-slip curves for the models are plotted in Figure 10. The load-slip curves for models 1and 2 are almost identical; however, the concrete tensile damage contours in Figure 11 show that concrete tensile cracking is more severe for the model with light reinforcement pattern. One possible explanation could be that cracking of concrete does not affect the frictional strength. Unlike shear studs bearing against concrete under shear, the strength of the clamping connectors relies on the normal force and the frictional coefficients, which are not varied significantly after the concrete has cracked, particularly because the cracking stems from the channels, not directly from the clamps. When cyclic loading is applied, the clamping connectors are not as ductile as under monotonic loading; the connectors retain approximately 70% of their strength after significant cyclic loading. By comparing the plots for models 1 and 4, it can be seen that the usage of shims reduces the clamping connector strength slightly. Large normal forces are generated at the frictional surfaces as a result of large bolt pretension, increasing the ultimate strength of the connectors in model 3 as compared to model 1.

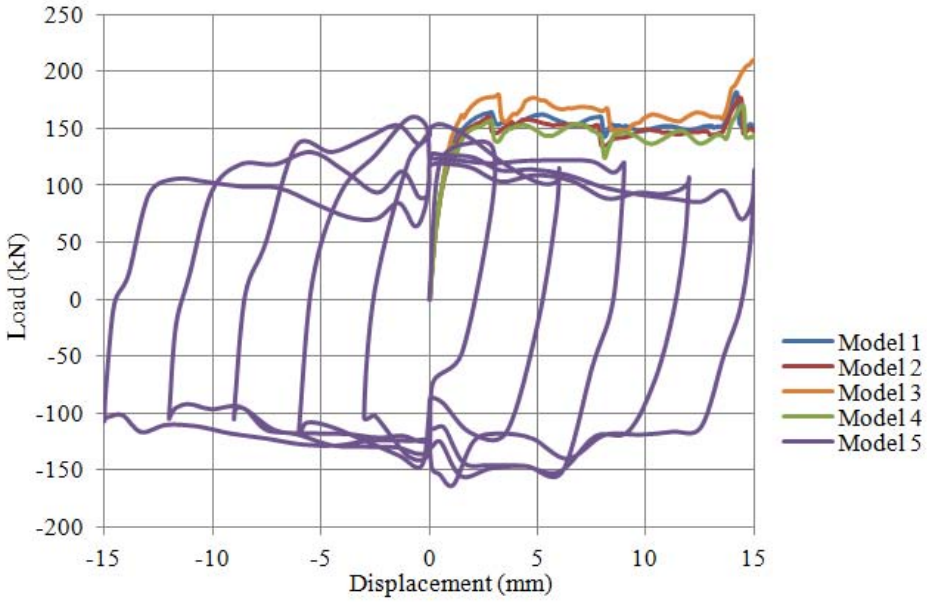

Figure 10. Load-slip curves for the computational models

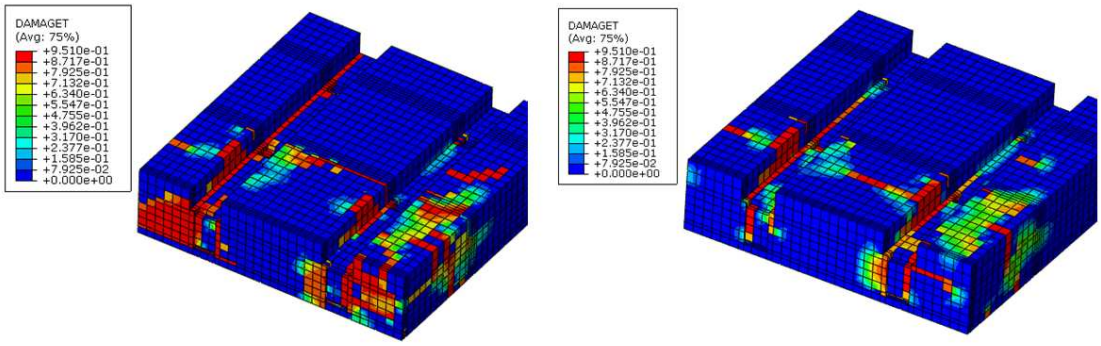

Figure 11. Concrete tensile damage D_t for models 1 and 2

CONCLUSIONS

A new deconstructable composite floor system, consisting of steel framing, precast concrete planks and clamping connectors, was presented herein. The proposed system has the potential not only to maintain the benefits offered by composite action and steel construction but also to enable refabrication and reuse of the components, closing the material flow loop and reducing resource consumption and waste in the construction industry.

A pushout test setup with two different reinforcement patterns was illustrated. A three-dimensional finite element model was then established to investigate the

behavior of the clamping connectors using a pushout test configuration. The model accounted for material nonlinearity and complex contact interactions. The load-slip curves presented ductile behavior of the clamping connectors, ensuring load redistribution comparable to that in composite beams could occur. The effects of various parameters on the load-slip curves were explored. Despite disparities in the concrete tensile damage contours for specimens with different reinforcement patterns, the influence on the ultimate strength of the clamping connectors was negligible. The connector strength was reduced slightly when shims were used, and it decreases when cyclic loading is applied.

ACKNOWLEDMENTS

This material is based upon work supported by the National Science Foundation under Grant No. CMMI-1200820, the American Institute of Steel Construction, Northeastern University, and Simpson Gumpertz & Heger. Any opinions, findings, and conclusions expressed in this material are those of the authors and do not necessarily reflect the views of the National Science Foundation or other sponsors.

REFERENCES

ABAQUS (2012). *Abaqus 6.12 Theory Manual*. Dassault Systèmes Simulia Corp., Providence, Rhode Island.

Anderson, N. S., and Meinheit, D. F. (2000). Design criteria for headed stud groups in shear: Part 1-Steel capacity and back edge effects. *PCI Journal*, 45(5), 46-75.

CEN (2004). *Eurocode 4: Design of Composite Steel and Concrete Structures, EN1994-1-1*, European Committee for Standardization, Brussels, Belgium.

Energy Information Administration (EIA) (2009). *Annual Energy Review*, U.S. Energy Information Administration, Washington, D.C.

Gattesco, N. and Giuriani, E. (1996). Experimental study on stud shear connectors subjected to cyclic loading. *Journal of Constructional Steel Research*, 38(1), 1-21.

GB50010-2002 (2002). *Code for Design of Concrete Structures*, Ministry of Housing and Urban–Rural Development, China.

Kulak, G. L., Fisher, J. W. and Struik, J. H (1987). *A Guide to Design Criteria for Bolted and Riveted Joints*, Wiley, NY.

Lam, D. (2000). New test for shear connectors in composite construction. *Composite Construction in Steel and Concrete IV*, ASCE, Reston, VA, 404-414.

Pavlović, M. et al. (2013). Bolted shear connectors vs. headed studs behaviour in push-out tests. *Journal of Constructional Steel Research*, 88, 134-149.

Saari, W. K., Hajjar, J. F., Schultz, A. E., and Shield, C. K. (2004). Behavior of shear studs in steel frames with reinforced concrete infill walls. *Journal of Constructional Steel Research*, 60(10), 1453-1480.